

Optics Letters

Retroreflective optical ISAC using OFDM: channel modeling and performance analysis

YUANXIN CUI,¹ CHEN CHEN,^{1,*} D YUEPING CAI,¹ ZHIHONG ZENG,¹ MIN LIU,¹ JIA YE,² SIHUA SHAO,^{3,5} AND HARALD HAAS⁴ D

Received 30 April 2024; revised 12 June 2024; accepted 9 July 2024; posted 10 July 2024; published 22 July 2024

In this Letter, we propose and investigate a retroreflective optical integrated sensing and communication (RO-ISAC) system using orthogonal frequency division multiplexing (OFDM) and corner cube reflector (CCR). To accurately model the reflected sensing channel of the RO-ISAC system, both a point source model and an area source model are proposed according to the two main types of light sources that are widely used. Detailed theoretical and experimental results are presented to verify the accuracy of the proposed channel models and evaluate the communication and sensing performance of the considered RO-ISAC system. © 2024 Optica Publishing Group. All rights, including for text and data mining (TDM), Artificial Intelligence (Al) training, and similar technologies, are reserved.

https://doi.org/10.1364/OL.528029

Optical wireless communication (OWC) using light-emitting diodes (LEDs) or laser diodes (LDs) has been widely envisioned as a promising enabling technology for the sixth generation (6G) of mobile networks, owing to its unique features such as abundant and license-free optical spectrum, robustness to electromagnetic interference, and inherent physical-layer security [1,2]. Considering the low-pass nature of practical OWC systems, many techniques have been applied to enhance the capacity of bandlimited OWC systems, e.g., spectral-efficient orthogonal frequency division multiplexing (OFDM) modulation [3], usable bandwidth extension [4,5], and multiple-input multiple-output (MIMO) transmission [6].

Besides communication capability, OWC systems can also be designed to realize sensing capability, and optical integrated sensing and communication (ISAC) technology has attracted great attention lately [7]. Compared with radio frequency (RF)-based ISAC systems, optical ISAC systems can fully utilize the large bandwidth of optical signals to achieve both high-speed communication and high-resolution sensing [8]. Since the communication and sensing performance is largely determined by the adopted waveforms in optical ISAC systems, several waveform designs have already been reported in the literature, such as pulse sequence sensing and pulse position

modulation (PSS–PPM) [9], combined linear frequency modulation and continuous phase modulation (LFM–CPM) [10], and pulse amplitude modulation (PAM)-based waveform [11]. To further improve the communication data rate, direct current-biased optical (DCO-OFDM) has also been applied in optical ISAC systems [12].

The key difference between conventional OWC systems and optical ISAC systems is the use of reflected light for an additional sensing purpose. Hence, the quality of the reflected light has a significant impact on the sensing performance. Compared with diffuse reflection at the target side, using a light reflector to enhance light reflection can substantially improve the quality of the reflected light for sensing. Although reflector-enhanced optical ISAC systems have already been considered in previous works such as [9,10], the accurate channel models for reflector-enhanced optical ISAC systems have not yet been developed so far. Moreover, the communication and sensing performance of optical ISAC systems with accurate channel models using different OFDM schemes still remains to be an open problem.

Aiming to address the above-mentioned issues, in this Letter, we propose and investigate a retroreflective optical ISAC (RO-ISAC) system using OFDM, where a corner cube reflector (CCR) is adopted to reflect the light at the target side. The selection of the CCR for light reflection is mainly due to its ability to concentrate and reflect the light back to the point where the light source locates at [13]. Accordingly, we propose both a point source model and an area source model for the CCR-based RO-ISAC systems. Moreover, two types of OFDM waveforms including DCO-OFDM and asymmetrically clipped optical OFDM (ACO-OFDM) are considered in the performance analysis. Detailed theoretical analysis and hardware experiments are carried out to evaluate the performance of the considered RO-ISAC systems.

Figure 1 depicts the schematic diagram of a RO-ISAC system using OFDM and CCR. At the RO-ISAC transceiver, the input bits are first utilized to perform OFDM modulation, and the resultant real-valued bipolar digital OFDM signal is further converted into an analog signal via digital-to-analog (D/A) conversion. Subsequently, a DC bias is added to ensure the

School of Microelectronics and Communication Engineering, Chongging University, Chongging 400044, China

²School of Electrical Engineering, Chongging University, Chongging, 400044, China

³Department of Electrical Engineering, Colorado School of Mines, Golden, Colorado 80104, USA

⁴Department of Engineering, University of Cambridge, 9 JJ Thomson Avenue, Cambridge CB3 0FA, UK

⁵sihua.shao@mines.edu

^{*}c.chen@cqu.edu.cn

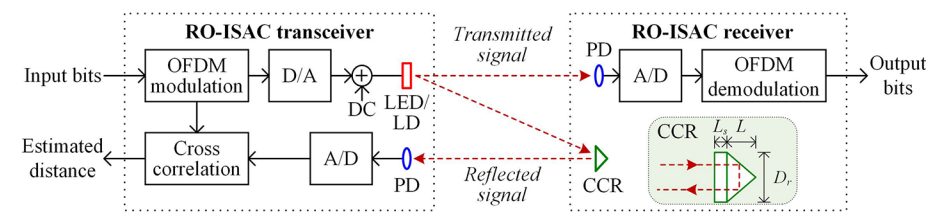


Fig. 1. Schematic diagram of a RO-ISAC system using OFDM and CCR. Inset in RO-ISAC transceiver shows the diagram of the CCR.

non-negativity of the generated OFDM signal. After that, the transmitted signal is obtained by modulating the intensity of the LED/LD light source with the electrical OFDM signal. At the RO-ISAC receiver, the transmitted signal is detected by the photo-detector (PD) to obtain the received electrical OFDM signal, which is further demodulated to recover the output bits, so as to fulfill the communication capability. Moreover, the RO-ISAC receiver is also equipped with a CCR to reflect the light back to the RO-ISAC transceiver. The inset in the RO-ISAC receiver shows the diagram of the CCR, where D_r , L, and L_s denote the diameter, the length, and the recessed length of the CCR, respectively [13].

At the RO-ISAC transceiver side, a PD is also used to detect the reflected signal, and the detected electrical analog OFDM signal is further converted into a digital signal via analog-todigital (A/D) conversion. Finally, cross correlation between the original OFDM signal and the reflected OFDM signal is executed to calculate and estimate the distance between the RO-ISAC transceiver and the RO-ISAC receiver, in order to fulfill the sensing capability. More specifically, we adopt the timedomain cross correlation method to perform ranging by using the time-domain samples of the original OFDM signal and the reflected OFDM signal. Considering the upsampling process during A/D conversion to obtain the digital time-domain samples of the reflected OFDM signal, the time-domain samples of the original OFDM signal should also be upsampled with the same upsampling rate before performing time-domain cross correlation. Letting α denote the upsampling rate, the maximum likelihood estimation of the time of flight can be represented by

$$\hat{\tau} = \arg\max_{\tau} \sum_{n=0}^{\alpha L_w - 1} y(n) x(n - \tau), \tag{1}$$

where x(n) and y(n) respectively denote the upsampled time-domain samples of the original OFDM signal and the time-domain samples of the reflected OFDM signal and L_w is the length of the selected time-domain window for cross correlation before upsampling. Hence, the estimated distance is given by $\hat{d} = c\hat{\tau}/2$, with c being the speed of light. Letting R_s denote the D/A sampling rate in the RO-ISAC transceiver, the ranging resolution and the maximum ranging distance are given by $\Delta d = c/2\alpha R_s$ and $d_{max} = c(\alpha L_w - 1)/2\alpha R_s$, respectively.

In practical RO-ISAC systems, the selection of a proper light source plays a vital role in achieving satisfactory communication and sensing performance. Generally speaking, an LD with a small divergence angle can be used to achieve long-distance communication and sensing, which however usually requires the assistance of an acquisition, tracking, and pointing (ATP) module to successfully establish a stable communication/sensing channel [9]. In contrast, an LED panel with a large divergence angle can be employed to obtain large-coverage communication

and sensing in a relatively short distance, which can work without ATP. Accordingly, both a point source model and an area source model are considered to establish the communication and sensing channel models for RO-ISAC systems in the following.

Figures 2(a) and 2(b) illustrate the RO-ISAC system with a point source model and an area source model, respectively. For the communication channel model, assuming the LED/LD light source follows the Lambertian emission pattern and only considering the line-of-sight (LOS) transmission, the communication channel gain can be expressed by [14]

$$h_c = \begin{cases} \frac{(m+1)A_c\rho_c}{2\pi d^2} \cos^m(\varphi)\kappa(\theta)\cos(\theta), & \text{for } 0 \le \theta \le \Phi_c\\ 0, & \text{else}, \end{cases}$$
 (2)

where $m=-\ln 2/\ln(\cos(\Psi))$ is the order of Lambertian emission with Ψ being the semi-angle at half power of the LED/LD light source; A_c and ρ_c are the active area and responsivity of the PD in the RO-ISAC receiver, respectively; d is the distance between the RO-ISAC transceiver and the RO-ISAC receiver; φ and θ are the irradiance angle and the incident angle, respectively; and $\kappa(\theta)=T_s(\theta)g(\theta)$, where $T_s(\theta)$ is the gain of optical filter and $g(\theta)=n^2/\sin^2(\Phi_c)$ is the gain of optical lens, with n and Φ_c denoting the refractive index and half-angle field of view (FOV) of the optical lens, respectively. It can be seen from Fig. 2 that the LOS communication channel model in Eq. (2) is applicable to both point source and area source models.

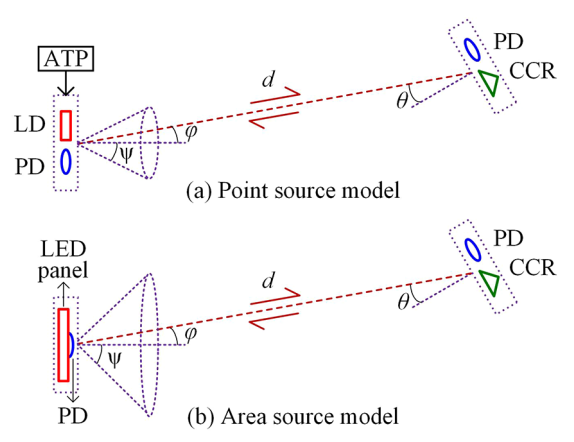


Fig. 2. Illustration of the RO-ISAC system with (a) a point source model and (b) an area source model.

Differing from the communication channel model, the sensing channel model might be different when different types of light sources are considered. For the point source model with ATP, as shown in Fig. 2(a), we can assume that the light emitted by the point source can always be fully reflected by the CCR, and

hence the sensing channel gain can be described by

$$h_s^{point} = \begin{cases} \frac{(m_p + 1)A_s\rho_s k}{8\pi d^2} \cos^{m_p + 1}(\varphi)\kappa(\varphi)\cos(\theta), \\ \text{for } 0 \le \theta \le \Phi_r \text{ and } 0 \le \varphi \le \Phi_s \end{cases}$$

$$0 \text{ else.}$$
(3)

where $m_p = -\ln 2/\ln(\cos(\Psi_p))$ is the corresponding Lambertian emission order and Ψ_p is the small semi-angle at half power of the point source, while A_s , ρ_s , and Φ_s are the active area, responsivity, and half-angle FOV of the PD in the RO-ISAC transceiver, respectively, and k and Φ_r are the reflectance and the half-angle FOV of the CCR in the RO-ISAC receiver, respectively. By comparing Eqs. (2) and (3), we can find that the distance is increased from d to 2d, and an additional $\cos(\varphi)$ term is included due to the incidence of the reflected signal to the PD in the RO-ISAC transceiver. Moreover, the term $\kappa(\varphi)$ should also be calculated with respect to φ .

For the area source model without ATP, as shown in Fig. 2(b), the light emitted by the area source cannot always be fully reflected by the CCR due to the orientation and the limited FOV of the CCR. As a result, the CCR might only be able to reflect part of the light emitted by the area source back to the PD in the RO-ISAC transceiver. Therefore, the sensing channel gain for the area source model can be modified as follows:

$$h_s^{area} = \begin{cases} \frac{(m_a + 1)A_s \rho_s k}{8\pi d^2} \cos^{m_a + 1}(\varphi) \kappa(\varphi) \cos(\theta) \xi(\varphi, \theta), \\ \text{for } 0 \le \theta \le \Phi_r \text{ and } 0 \le \varphi \le \Phi_s \\ 0, \text{ else,} \end{cases}$$
(4)

where $m_a = -\ln 2/\ln(\cos(\Psi_a))$ is the Lambertian emission order and Ψ_a is the large semi-angle at half power of the area source and $\xi(\varphi,\theta)$ denotes the effective reflecting ratio of the CCR with respect to the area source. Assuming the PD is embedded in the area source and letting A_{light} and A_{PD} respectively denote the areas of the area source and the overall PD device, the effective reflecting ratio $\xi(\varphi,\theta)$ can be defined by

$$\xi(\varphi,\theta) = \frac{A_{eff}(\varphi,\theta)}{A_{light} - A_{PD}},$$
(5)

where $A_{eff}(\varphi, \theta)$ is the effective reflecting area of the CCR with respect to the area source, and it can be approximated by [13]

$$A_{eff}(\varphi,\theta) = \frac{2r_k^2}{\cos(\varphi)}(\cos^{-1}\left(\frac{2(L+L_s)\tan(\theta)}{r_k}\right) - \frac{2(L+L_s)\tan(\theta)}{r_k}\sqrt{r_k^2 - 2(L+L_s)\tan(\theta)^2}) - \frac{A_{PD}}{\cos(\varphi)},$$
(6)

where r_k is a coefficient determined by both the CCR and the PD, which can be approximated by $r_k = D_r + L_{PD}/2$ with L_{PD} denoting the side length of the square-shaped PD.

To evaluate the performance of the proposed channel models and further analyze the performance of the RO-ISAC system using OFDM and CCR, we conduct theoretical analysis and proof-of-concept experiments in the following. For simplicity and without loss of generality, we assume that the light source in the RO-ISAC transceiver faces toward the RO-ISAC receiver, i.e., the angle of irradiance from the light source is $\varphi=0^\circ$, and we focus on the impact of the incident angle to CCR on the performance of the proposed channel models. The other parameters in the theoretical analysis are given as follows: $c=0^\circ$

 3×10^8 m/s, $\Psi_p = 10.5^\circ$, $\Psi_a = 65^\circ$, $\Psi_r = 30^\circ$, $\Psi_c = \Psi_s = 65^\circ$, $L_w = 256$, $D_r = 50$ mm, L = 35.7 mm, $L_s = 6.3$ mm, k = 0.92, $\rho_c = \rho_s = 0.25$ A/W, $L_{PD} = 10$ mm, n = 1.51, and $T_s(\theta) = 0.9$.

Figure 3 shows the theoretical sensing channel gain versus the incident angle to CCR for both point and area sources. For both types of light sources, the sensing channel gain is greatly reduced when the distance is increased. Moreover, the sensing channel gain for the area source is significantly lower than that for the point source, which is mainly because the area source has a much larger divergence angle than that of the point source. Furthermore, the sensing channel gain for the area source is much more sensitive than that for the point source, which is rapidly reduced when increasing the CCR incident angle.

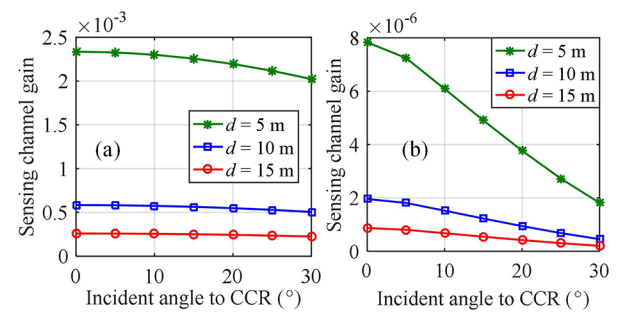


Fig. 3. Theoretical sensing channel gain versus incident angle to CCR for (a) a point source and (b) an area source.

To verify the accuracy of the proposed area source channel model, an experimental setup in Fig. 4 is established for sensing channel gain measurement using an LED panel as an area source. In the experiments, the CCR faces toward the LED panel with a distance of 70 cm, where two CCRs with diameters of 50 and 24.5 mm and two PDs with side lengths of 10 and 3.6 mm

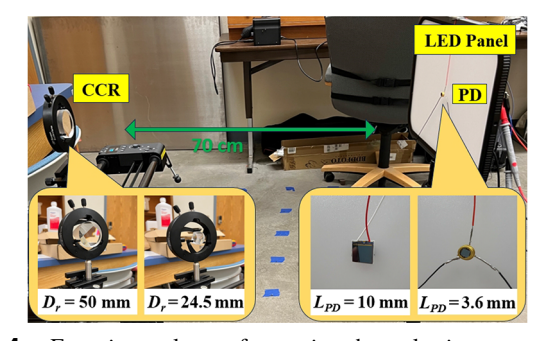


Fig. 4. Experimental setup for sensing channel gain measurement using an LED panel as an area source.

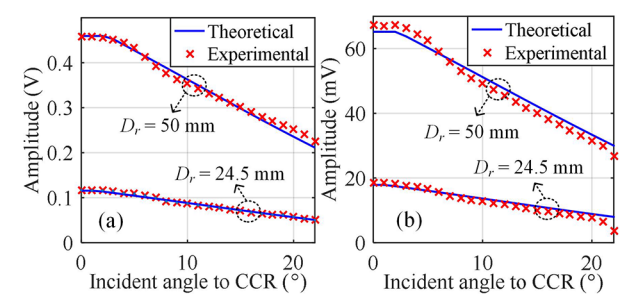


Fig. 5. Theoretical and experimental sensing channel gain versus incident angle to CCR for an area source with a PD side length of (a) $L_{PD} = 10$ mm and (b) $L_{PD} = 3.6$ mm.

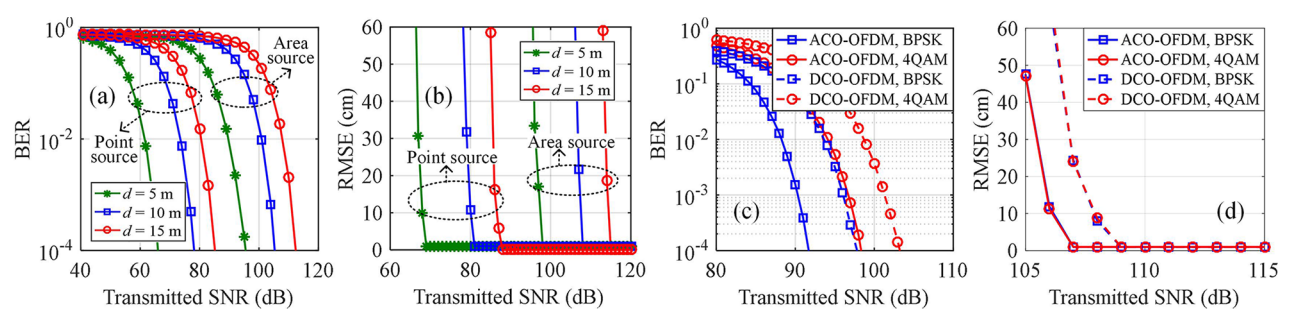


Fig. 6. Theoretical results of (a) BER versus transmitted SNR using DCO-OFDM with 4QAM, (b) ranging RMSE versus transmitted SNR using DCO-OFDM with 4QAM, (c) BER versus transmitted SNR for a distance of 10 m, and (d) ranging RMSE versus transmitted SNR for a distance of 10 m.

are considered. Figure 5 shows the theoretical and experimental sensing channel gain versus the incident angle to CCR for the area source. It can be seen that a higher sensing channel gain is obtained when the CCR with a larger diameter or the PD with a larger side length is used. Moreover, it can also be clearly observed that the experimental results closely match the theoretical results predicted by Eq. (4), showing the high accuracy of the proposed area source channel model.

We further analyze the theoretical communication and sensing performance of the RO-ISAC system using the proposed channel models, where we assume $\varphi = \theta = 0^{\circ}$, $R_s = 1$ GSa/s, and $\alpha = 5$. Hence, the ranging resolution and the maximum ranging distance are 3 cm and 38.4 m, respectively. Moreover, the noise of the RO-ISAC system is assumed to be real-valued zero-mean additive white Gaussian noise (AWGN), which has a power of $P_n = N_0 B$, with N_0 and B denoting the noise power spectral density and bandwidth, respectively. Both DCO-OFDM and ACO-OFDM modulation schemes are applied in the RO-ISAC system. For a bandwidth B, the transmission rates of DCO-OFDM and ACO-OFDM using M-ary constellation are given by $B \log_2 M$ and $\frac{B}{2} \log_2 M$, respectively. In the following analysis, we assume $N_0 = 10^{-22} \,\text{A}^2/\text{Hz}$ and $B = 20 \,\text{MHz}$ [6], and both binary phase-shift keying (BPSK) and 4-ary quadrature amplitude modulation (4QAM) constellations are considered.

Figure 6(a) shows the BER versus the transmitted signal-tonoise ratio (SNR) for point and area sources using DCO-OFDM with 4QAM, where the transmitted SNR is defined as the ratio of the transmitted electrical signal power to the additive noise power [6]. It is evident that a longer distance yields a higher BER, and the BER performance for a point source is much better than that for an area source. The root mean square error (RMSE) of ranging using DCO-OFDM with 4QAM is shown in Fig. 6(b), where a larger RMSE is obtained at a longer distance and the ranging RMSE for a point source is much smaller than that for an area source. Figures 6(c) and 6(d) compare the communication and ranging performance of DCO-OFDM and ACO-OFDM with both BPSK and 4QAM constellations at a distance of 10 m. In terms of communication, ACO-OFDM generally achieves better BER than DCO-OFDM when using the same constellation. In terms of ranging, the use of different constellations has a negligible impact on the RMSE, but the selection of OFDM format can greatly affect the RMSE. Specifically, for a transmitted SNR of 107 dB, the RMSEs using DCO-OFDM and ACO-OFDM are about 24 m and 1 cm, respectively, demonstrating the superior ranging performance of ACO-OFDM in comparison to DCO-OFDM.

In this Letter, using OFDM and CCR has been investigated. Particularly, two channel models, including a point source model and an area source model, have been proposed to model the reflected sensing channel of the RO-ISAC system. Moreover, the detailed theoretical and experimental results have been proposed to model the reflected sensing channel. The obtained results show a good match between the experimentally measured channel gains and the theoretically prediction channel gains, suggesting the high accuracy of the proposed channel models. It is also revealed that ACO-OFDM can achieve better ranging performance than DCO-OFDM in the RO-ISAC system. Therefore, the theoretical and experimental results of this work might be useful for the design and implementation of RO-ISAC systems in practical applications.

Funding. National Natural Science Foundation of China (62271091); Natural Science Foundation of Chongqing Municipality (cstc2021jcyj-msxmX0480); National Science Foundation (CNS-2245747).

Disclosures. The authors declare no conflicts of interest.

Data availability. Data underlying the results presented in this Letter are not publicly available at this time but may be obtained from the authors upon reasonable request.

REFERENCES

- 1. N. Chi, Y. Zhou, Y. Wei, et al., IEEE Veh. Technol. Mag. 15, 93 (2020).
- Z. Wei, Z. Wang, J. Zhang, et al., Prog. Quantum Electron. 83, 100398 (2022).
- R. Mesleh, H. Elgala, and H. Haas, J. Opt. Commun. Netw. 3, 620 (2011).
- 4. J. Shi, W. Xiao, Y. Ha, et al., Opt. Express 30, 33337 (2022).
- 5. J. Chen, B. Deng, C. Chen, *et al.*, Opt. Express **31**, 30723 (2023).
- C. Chen, X. Zhong, S. Fu, et al., J. Lightwave Technol. 39, 6063 (2021)
- S. Wang and H. Chen, in *International Symposium on Modeling and Optimization in Mobile, Ad Hoc, and Wireless Networks (WiOpt)* (2023), pp. 207–214.
- 8. C. Liang, J. Li, S. Liu, et al., Digit Signal Process 145, 104340 (2024).
- 9. Y. Wen, F. Yang, J. Song, et al., IEEE Commun. Lett. 27, 1525 (2023).
- 10. Y. Wen, F. Yang, J. Song, et al., IEEE Commun. Lett 28, 43 (2024).
- J. Wang, N. Huang, C. Gong, et al., IEEE Internet Things J. 1, 1 (2024).
- E. B. Muller, V. N. Silva, P. P. Monteiro, et al., IEEE Photonics Technol. Lett. 34, 757 (2022).
- S. Shao, A. Salustri, A. Khreishah, et al., IEEE Internet Things J. 10, 11429 (2023).
- T. Komine and M. Nakagawa, IEEE Trans. Consumer Electron. 50, 100 (2004).